The seasonal cycle of planetary boundary layer depth determined using COSMIC radio occultation data

Ka Man Chan and Robert Wood

Department of Atmospheric Science, University of Washington, Seattle WA

Abstract.

The seasonal cycle of planetary boundary layer (PBL) depth is examined globally using observations from the Constellation Observing System for the Meteorology, Ionosphere, and Climate (COSMIC) satellite mission. COSMIC uses GPS Radio Occultation (GPS-RO) to derive the vertical profile of refractivity at high vertical resolution (~100 m). Here, we describe an algorithm to determine PBL top height and thus PBL depth from the maximum vertical gradient of refractivity. PBL top detection is sensitive to hydrolapses at non-polar latitudes but to both hydrolapses and temperature jumps in polar regions. The PBL depths and their seasonal cycles compare favorably with selected radiosonde-derived estimates at Tropical, midlatitude and Antarctic sites, adding confidence that COSMIC can effectively provide estimates of seasonal cycles globally. PBL depth over extratropical land regions peaks during summer consistent with weak static stability and strong surface sensible heating. The subtropics and Tropics exhibit a markedly different cycle that largely follows the seasonal march of the intertropical convergence zone (ITCZ) with the deepest PBLs associated with dry phases, again suggestive that surface sensible heating deepens the PBL and that wet periods exhibit shallower PBLs.

Marine PBL depth has a somewhat similar seasonal march to that over continents but is weaker in amplitude and is shifted poleward. The maximum seasonal amplitude over oceans occurs over the Arctic. Over subtropical/tropical oceans there is seasonal asymmetry about the equator, with winter maxima in the Northern Hemisphere but fall maxima in the south. The seasonal march of PBL depth is largely modulated by the seasonal cycle of static stability in the extratropics and by the monsoon circulations at tropical and subtropical latitudes.

1. Introduction

The planetary boundary layer (PBL) is the lowest part of the troposphere that is directly influenced by the Earth’s surface through the exchange of heat, momentum and moisture (Stull 1988, Arya 2009). The depth of the PBL sets limits for the mixing height of important surface-emitted constituents and is a primary determinant of cloud type and coverage that affect the Earth’s radiation budget (Wood 2012). It is therefore critical to gain an understanding of the spatiotemporal variability of the PBL depth.

The PBL top generally is marked by sharp gradients in one or more of the following: humidity; temperature; turbulence; wind; tracers including aerosol particles or boundary layer cloud droplets. These gradients are detectable using measurements from radiosondes, and surface and spaceborne remote sensors. These provide a means to estimate the depth of the PBL. Spaceborne remote sensing of the PBL is attractive because it offers the potential to provide global statistics regarding the spatial and temporal variability of the PBL depth.

Recently, there have been a number of studies that have used spaceborne remote sensing to generate regional and global climatologies of the PBL depth. These studies have used a number of different techniques to identify the top of the PBL. The first set of studies uses thermal infrared brightness temperatures to determine the temperature T_{top} at the top marine stratus and stratocumulus clouds. Because the temperature profile in the PBL does not depart dramatically from a dry adiabat, and because over most of the ocean the air-sea temperature difference is small (Wood and Bretherton 2004), one can use T_{top} and sea-surface temperature estimates from satellites to estimate PBL depth. Heck et al. (1990) and Minnis et al. (1992) pioneered these estimates, with later refinement to account for variations in PBL stratification by Wood and Bretherton (2004) and Zuidema et al. (2009). In terms of utility for climatological study, these estimates are limited to regions where unbroken clouds dominate. They do not work well over land or for regions where shallow cumulus are prevalent. One variation on this type of estimate uses a direct estimate of cloud top height from multi-angle imaging (Karlsson et al. 2010) instead of indirect estimation from T_{top}. Another uses spaceborne lidar to estimate PBL top through the examination of cloud top heights (Wu et al. 2008). All methods that use cloud top height face the same problems as the infrared approach for estimating PBL top height in regions of broken clouds whose tops do not always lie at the top of the PBL (Karlsson et al. 2010).

A second approach uses the backscatter from aerosol particles to determine the PBL depth using spaceborne lidar. Because many of the particles responsible for light scattering are emitted from the Earth's surface (e.g., sea-salt, dust and soil particles), these particles are often confined within the PBL. The PBL top is often marked by a sharp decrease in aerosol scattering that may be detected from space (Randall et al. 1998). This approach has been used in a number of recent studies to characterize the PBL depth over the oceans (Palm et al. 2005), land (McGrath-Spangler and Denning 2012) and globally (McGrath-Spangler and Denning, 2013).

Meteorological definitions of the PBL top generally involve stability/bulk Richardson number criteria to identify a statically stable layer atop the PBL. These have generally been applied to radiosonde datasets (and sometimes wind profilers) that have fine vertical resolution measurements of temperature (Seidel et al. 2010), from which regional climatologies have been produced (Seidel et al. 2012). However, this approach is not well-suited to application to vertical temperature profiles from most passive spaceborne sounders (infrared and microwave) because the vertical resolution of the passively-retrieved profiles is at best 1-2 km. This is a very coarse resolution with which to estimate PBL top height, for which variations of only a few hundred meters have important implications (Wood and Bretherton 2004).

Temperature profiles from limb sounders, however, have the potential for higher vertical resolution, making this technique much more attractive for use in PBL depth detection. Indeed, spaceborne Global Positioning System radio occultation (GPS-RO) provides refractivity profiles with high vertical resolution making this approach attractive for use in identifying sharp vertical gradients and hence PBL top (Kursinski et al. 1997, Hajj et al. 2004). Refractivity is a function of temperature, pressure and water vapor (Kursinski et al. 1997), with no significant dependence upon cloud or rain water. The first GPS-RO satellite mission was the MicroLab I that began making measurements 1995 (Kursinski et. al. 1997). Since 2006, COSMIC, a joint Taiwan-United States mission, has used six LEO satellites to provide GPS-RO observations for use in weather forecasting with much better sampling than previous missions (Anthes et al. 2008). The GPS-RO LEO satellites receive radio signals passing through Earth’s atmosphere from GPS satellites and calculate the bending angle from the phase and amplitude of the signals as the signal is attenuated by the atmosphere during occultation events. The bending angle is then converted, using an Abel inversion technique (Sokolovskiy 2001) into a vertical refractivity profile that depends upon atmospheric density and the partial pressure of water vapor (Bean and Dutton 1968). COSMIC provides vertical profiles of refractivity at 100 m vertical resolution throughout the troposphere.

Several studies have used GPS-RO to estimate PBL top height. Von Engeln et al. (2005) first used the height at which superrefraction results in GPS-RO signal loss as a means to determine the height of the inversion. Sokolovskiy et al. (2006) showed that this approach can lead to false PBL top height detections in some cases and developed an improved approach that uses an open loop tracking technique (see Sokolovskiy 2001) to allow tracking the GPS-RO signal significantly further down into the lower troposphere. This allows a more precise estimate of the height of strongest vertical refractivity gradient that marks the PBL top (Sokolovskiy et al. 2006).

Climatological estimates of PBL depth over oceans based on this approach were made by Guo et al. (2011) and Ao et al. (2012). The results are consistent, showing deep PBLs over the warmer parts of the subtropical ocean and generally shallower PBLs over the extratropical and cold eastern subtropical oceans. Both studies present some aspects of the seasonal cycle of PBL depth. For example, Ao et al. (2012) explored the seasonal cycle of PBL depth over the Sahara region, and Guo et al. (2011) presented global maps for different seasons. However, the seasonal cycle was not a primary motivation of these studies and so there is considerable scope to examine the seasonal march of PBL depth from GPS-RO. That is the primary purpose of this paper, which uses a similar approach applied to data from COSMIC to explore the seasonal march of PBL depth over the global land and oceans.

In this paper, section 2 describes PBL top detection algorithms based on those introduced by Guo et al. (2011), which we develop and modify. Both approaches use minima in the vertical refractivity gradient to determine the height of the PBL top, but each has a different screening approach to ensure distinctness of the minima. Section 2 also describes how the algorithms are applied to radiosonde soundings as a means to compare with the COSMIC seasonal cycle estimates. Section 3 then presents a global analysis of the seasonal march of PBL depth from COSMIC, with Section 4 providing an assessment of the relative importance of moisture and temperature gradients to the PBLs detected here. Section 5 examines the sharpness of the detected PBLs and examines its seasonality. Section 6 provides a brief discussion and conclusions.

2. Methodology

2.1 Data Sources

2.1.1 COSMIC Observations

Global Positioning System radio occultation (GPS-RO) data from the Constellation Observing System for the Meteorology, Ionosphere, and Climate (COSMIC) mission is the primary dataset used in this study. The data were obtained from the COSMIC RO Data Analysis and Archive Center[1] (DAAC) hosted by the University Corporation for Atmospheric Research (UCAR). Here, we use all available profiles from five complete years (2007-2011) to ensure acceptable statistical reliability of the seasonal cycles (see section 3). COSMIC provides ~1500 profiles distributed over the globe each day.

For the analysis presented here, only the vertical profile of refractivity N is used in the PBL top detection algorithm (section 2.2). The vertical resolution of the profile is a constant 100 m. After the algorithm is applied, the processed data are gridded into monthly and seasonal (three-monthly: DJF, MAM, JJA, SON) grids at 5×5° spatial resolution. From the gridded statistics we derive the mean and the monthly and seasonal anomalies of PBL depth, the standard errors, and also mean values of the sharpness parameter (following Ao et al. 2012, see also section 5 below) and the frequency at which a PBL top is detected. The global grids then are smoothed using a five-point smoothing weighted by the frequency of PBL top in the central and adjacent four grid points. The quasi-random COSMIC sampling over the Earth ensures good sampling throughout the year with samples available at all local times, ensuring little diurnal sampling bias.

---

[1] http://cdaac-www.cosmic.ucar.edu/cdaac/index.html

Not every GPS-RO occultation can be tracked to the surface due to terrain and signal distortion in the atmosphere due primarily to water vapor variability along the line of sight. For this study we only use COSMIC soundings that extend below 500 m above the surface to attempt to mitigate undersampling of shallower PBLs and consequential biased statistics. Figure 1 shows the number of COSMIC GPS-RO profiles in each 5×5° box meeting this criterion during the entire period (2007-2011), indicating a large number of available profiles over the ocean and flat land terrain. In these regions, there are usually in excess of 50 retrievals per composite month for each box, i.e. more than 600 retrievals in total. Low numbers of suitable profiles are available in the Tropics, in high polar regions, and over mountain ranges (Fig. 1). In the Tropics, high moisture levels and moisture spatial variability results in difficulties tracking the signals down to the near-surface (Ao et al. 2012), whereas high polar regions have fewer profiles per 5×5° box because box area decreases significantly rather than there being physical reasons.

2.1.2 Radiosonde Observations

Radiosonde soundings are used to compare with the seasonal PBL depth estimates from COSMIC. We use soundings from six stations to cover a range of locations in the Tropics, midlatitudes and high latitude regions (Table 1). The mean and seasonal cycles of PBL depth are derived from the radiosondes using the COSMIC algorithm (see section 2.2) applied to the refractivity derived from each sounding separately (using pressure, temperature and humidity following Eqn. 1 below). All radiosonde data other than from Hong Kong are taken at high temporal resolution (6 seconds at Annette, St.Paul and Hilo, and 10 seconds at Macquarie and Halley). This resolution translates into a vertical resolution of 30-50 m. Hong Kong soundings are at a lower vertical resolution typically averaging ~200 m at altitudes below 5 km. The PBL depths from the radiosondes are grouped into composite monthly means for comparison with the COSMIC mean and seasonal cycle estimates, as described in section 2.3.

To derive statistically robust seasonal cycles from the radiosondes, multiple years of soundings are used. The sounding data were obtained from three sources: Stratospheric Processes and their Role in Climate (SPARC[1]); the British Atmospheric Data Centre (BADC[2]); the University of Wyoming (UWYO[3]) We are not able to use the same time period as that over which the COSMIC estimates are made because high resolution soundings from SPARC are only available from 1998-2008. However, because we are here focusing on the seasonal cycle, we do not expect a significant impact from our exact choice of years. Two radiosondes are launched every day one hour prior to the official observation times (00 UTC and 12 UTC). We use both sounding times to minimize diurnal impacts on the comparisons.

2.1.3 Reanalysis data

To establish the relationship between the seasonality in PBL depth and that in large scale meteorology, we use NCEP reanalysis data. In this study, we use the reanalysis data to determine monthly climatological mean values of inversion strength (EIS) metric of Wood and Bretherton (2006). EIS is a modified form of the lower tropospheric static stability (LTS) metric defined by Klein and Hartmann (1993) that is the difference between the potential temperature at 700 hPa and that near the surface, but EIS takes into account the observed finding that the free-tropospheric profile is quite close to a moist adiabat (Wood and Bretherton 2006). Thus EIS is a more appropriate measure of the strength of the PBL capping inversion than is LTS under moist processes. Our choice to examine the seasonality of EIS is motivated by the finding from an

---

[1] http://www.sparc.sunysb.edu/html/hres.html)
[2] http://badc.nerc.ac.uk/home/index.html
[3] http://weather.uwyo.edu/upperair/sounding.html

analysis of the PBL depth in a GCM that static stability plays a major role in determining geographical variability in PBL depth (Medeiros et al. 2005). Here, EIS is derived from the potential temperature at 700 hPa and at the surface, using the monthly long term mean NCEP reanalysis data at these levels.

2.2 Algorithm for automatic detection of PBL top

The PBL top is usually marked by a sudden sharp change or discontinuity of temperature, water vapor pressure, or both, both of which impact the refractivity gradient. The refractivity is sensitive to the vertical gradient water vapor pressure p_w [hPa], pressure p [hPa], and temperature T [K], via the relation (Bean and Dutton 1968, Kursinski et al. 1997):

$$N = a\frac{p}{T} + b\frac{p_w}{T^2} \qquad [1]$$

where $a = 77.6$ N-units K $(\text{hPa})^{-1}$ and $b = 3.77\times10^5$ N-units K^2 $(\text{hPa})^{-1}$.

The algorithm identifies the PBL top as a layer with the most negative minimum in the vertical gradient of refractivity $N' = dN/dz$, building on the approach described in Guo et al. (2011). Following Sokolovskiy et al. (2006) and Guo et al. (2011), we apply a fixed-width (300 m) sliding-window linear regression on $N(z)$ to determine N' in order to reduce noise, i.e.:

$$N(z) = N'z + B \qquad [2]$$

As we show in section 4, in most regions other than the high polar regions, the moisture gradient at the PBL top (the second term in Eqn. 1) contributes most significantly to N'. Ao et al. (2012) found this to be the case when they compared estimates from refractivity profiles with those from moisture profiles derived from COSMIC. However, at very cold temperatures in the high polar regions, p_w is low and we find that the temperature increase actually contributes most to the minimum in N' (section 4).

Simply diagnosing the PBL top height based on the height at which $N' = \min[N']$ is insufficient, however, because there can be multiple minima in N', some of which may be only marginally weaker than $\min[N']$. We apply most of the constraints used by Guo et al. (2011), which focused on detecting sharp-topped PBLs, and we add additional constraints to deal with noise in the N profiles. The detected PBL depth h meets the following criteria:

a) h is the height at which $N'(h) = \min[N']$;

b) $N'(h) < -50$ (N units) km^{-1}. In other words, the minimum has to be a sharp one. This is the same sharpness constraint used in Guo et al. (2011);

c) $h < 3.5$ km above the surface. This avoids contamination by mid-level inversions;

d) h is only defined if there are fewer than seven minima in the N profile. A high number of local minima usually indicates a poorly-defined PBL;

e) If there are two or more minima with values within 20% of each other, no h is determined.

f) The ratio of relative *distinctness* of the minima $N' \geq 1.25$, where *distinctness* is defined as the ratio of $\min[N']$ to the *mean* of the local minima. In other words, to be classified as a PBL top, the minimum in refractivity gradient must be sufficiently distinct from other local minima.

The PBL detection frequency (Fig. 2) is the percentage of profiles extending down to below 500 m above the surface for which a PBL top is determined. Values are generally consistent with those presented in Guo et al. (2011), with the highest frequencies in a subtropical band where values exceed 40%. The highest frequencies of all are found over the cold eastern subtropical oceans. High frequencies are also found over the extratropical oceans, whereas low values are found over the poles and the warm Tropical regions, where PBL occurrence frequencies are below 20%. The subtropical bands of high PBL detection frequency extend further poleward during summertime and equatorward in winter (Fig. 3), consistent with strengthening and weakening of the Hadley cell (Dima and Wallace 2003). In addition to the subtropical meandering of the PBL detection frequency, over the northern extratropical oceans there is strong seasonal variability that is not evident over the Southern Ocean (Fig. 3).

2.3 Comparison of radiosonde and COSMIC PBL depth seasonal cycles.

To evaluate the quality of COSMIC PBL depth estimates and their seasonal variations, we compare with radiosonde estimates at the six sites (section 2.1.2, Table 1). To do this, we use monthly mean smoothed PBL depths from each 5×5° box within which the radiosonde station is situated (section 2.1.1). Sampling error estimates are determined by assuming that each COSMIC and each radiosonde PBL depth estimate is independent of all the others. The correlation coefficient between the seasonal cycles is derived from the monthly composite means. The annual mean PBL depths estimated by COSMIC and the radiosondes agree to within about 0.2 km at all the stations and the means have a correlation coefficient of 0.97 across the stations (Table 2). This clearly shows that COSMIC can reproduce the annual mean PBL depths estimated from radiosondes given the sampling period of several years used here.

The seasonal cycle time series for the two estimates agree well for four of the sites (St. Paul, Macquarie Island, Hong Kong and Halley are 0.6 or better, Fig. 4 and Table 3), especially given that the sampling uncertainties in the monthly mean estimates are a significant fraction of the seasonal amplitude. Seasonal cycles from the radiosondes and COSMIC are positively correlated at Annette and Hilo, but the correlations are weaker and are not statistically significant at the 95% level. The months of max and min departure from the annual mean agree to within a month or two for the three well-correlated sites, but not surprisingly there is little agreement for the other two sites. The results highlight that determining a seasonal cycle using data from a single radiosonde station or from a 5×5° COSMIC averaging box is challenging given the sampling uncertainties. Nevertheless, the good agreement at three of the six sites would not be expected by chance. We used bootstrap sampling of seasonal cycles drawn entirely randomly from normal distributions to demonstrate that the likelihood of obtaining even a single seasonal cycle that is correlated with $r > 0.6$ has a probability of only 0.02, and therefore the likelihood of obtaining three out of six correlation coefficients above 0.6 by random chance is vanishingly small.

Although the seasonal correlation coefficients are not universally high, the agreement in the amplitude of the seasonal cycles seen by COSMIC and the radiosondes at all the sites is rather good, with a correlation coefficient of 0.99 between the maximum absolute deviations (Table 3) across the stations. The seasonal amplitude is largest at Hong Kong where it exceeds 0.5 km (a seasonal range of ~1 km), followed by St. Paul, Hilo and Halley where it is ~0.25-0.3 km, while it is considerably lower at Macquarie. This is particularly interesting because St. Paul and Macquarie are both midlatitude remote marine locations away from the continental landmasses at approximately the same latitude from the Equator (Table 1). As we will see, this difference in seasonal cycle amplitude over the oceans is not peculiar to these sites but is a robust hemispheric feature. It is also interesting that at St. Paul and Macquarie (at 57°N and 55°S respectively), the PBL depth is maximal during late summer whereas at Hong Kong (~22°N) it is minimal during summer.

3. Global analysis of seasonal variability of PBL depth

Figure 5 presents the global annual mean PBL depth from COSMIC for the 2007-2011 period. In the annual mean, PBL depths are lowest (<1 km) over high latitudes and highest (~2 km) over the subtropics and tropical trades, with additional minima (~1.4 km) over the maritime continent and over the cold eastern subtropical oceans. Particularly deep (>1.8 km) marine PBLs occur over the South Atlantic east of Brazil, the Gulf of Aden and over the western Indian Ocean. Over continents in the subtropics and Tropics, the PBL depth is typically greater over arid regions and lower over regions with abundant surface moisture. The sampling error for the annual mean PBL depths (Fig. 6), estimated assuming each COSMIC PBL depth estimate within the 5×5° grid box is independent, are < 0.1 km over the cold eastern subtropical oceans (see also Xie et al. 2012), ~0.1 km over the extratropical oceans, ~0.15-0.2 km over arid land areas, and are as high as 0.3 km over the warm tropical oceans and land areas. This means that the geographical variations described above are statistically robust. The sampling error is to a large extent determined by the product of the frequency of PBL top detection (Fig. 2) and the number of retrievals penetrating to below 500 m above the surface (Fig. 1), but the spatiotemporal variability of the PBL depth also contributes, especially during the wet seasons in the subtropical/tropical regions.

The annual mean climatology agrees very well with previous open loop GPS RO estimates from COSMIC (Guo et al., 2011; Ao et al., 2012), but this is not very surprising given that our method is very similar to that in used in the previous COSMIC studies. Over regions of extensive subtropical low cloud, there is very good agreement between our COSMIC PBL depth climatology and that derived from cloud top temperature (Wood and Bretherton 2004, Zuidema et al. 2009), with PBL depth increasing as one moves westward from the cold waters off the western subtropical continental margins to the warmer waters further westward and equatorward (see also Fig. 10 in Wyant et al. 2010).

The COSMIC PBL depths over ocean do not compare particularly well with those from spaceborne lidar (McGrath-Spangler and Denning 2013), whose mean depths over ocean are everywhere lower than 1 km. In addition, the lidar estimates over ocean shown only weak latitudinal gradients compared with COSMIC (compare our Fig. 5 with Fig. 3 in McGrath-Spangler and Denning 2013). There is a straightforward reason for the discrepancy, however. COSMIC is primarily sensitive to the hydrolapse (section 4), whereas the lidar estimates are picking up cloud top height and sharp drop-offs in aerosol scattering. Although cloud top height is close to the hydrolapse over regions of extensive marine stratocumulus (Caldwell et al. 2005), this is not the case when the PBL is not well-mixed (Karlsson et al. 2011), which is the case over a considerable fraction of the ocean (Wood and Bretherton 2004). Further, the aerosol drop-off typically occurs at the top of the surface mixed layer rather than at the top of the decoupled layer that marks the top of the trade wind layer over the subtropical and tropical oceans (Wu et al. 2008, Tackett and Di Girolamo 2009), above which the moisture decreases sharply (Albrecht et al. 1995). It is a matter of definition whether one considers the top of the surface mixed layer or the deeper trade layer to be the top of the PBL, and therefore one must be cautious comparing PBL depth estimates that use very different techniques.

Seidel et al. (2010, 2012) explore methods to determine PBL depth and then derive a climatology from radiosonde data over the continental United States and Europe based upon a Richardson number stability criterion to detect PBL top. Our COSMIC estimates, which primarily detect hydrolapse features apart from in the high polar latitudes (see section 4), are best compared with the Seidel et al. values during daytime, because the nocturnal PBLs based on stability tend to form *within* the residual moist layer left over from mixing during the day. Annual mean values of PBL depth at 12 UTC (close to local noon) over Europe are ~1 km (Seidel et al. 2010, 2012), which are somewhat lower than the COSMIC estimates (Fig. 5). This difference most likely reflects the different information provided by stability-based and moisture-based methods of estimating the height of the PBL top (Seidel et al. 2010).

The COSMIC PBL depth observations are broadly consistent with values diagnosed from a general circulation model with a mixed-layer representation of the PBL (Medeiros et al. 2005). In that study, PBL depth was found to be controlled largely by static stability and surface fluxes, an issue we will return to when analyzing the seasonal cycle.

Figure 7 shows seasonal mean departures of PBL depth from the annual mean, and clearly reveal coherent patterns of seasonal PBL variability. In most locations, anomalies are strongest in the winter and summer and are weaker in spring and fall. There is a remarkable contrast in both phase and amplitude between the seasonality at extratropical latitudes (>40°) compared with that at subtropical/tropical (Hadley cell) latitudes (35°S-35°N), and so we will discuss each separately.

3.1 Extratropical seasonal variability

In contrast to the annual mean PBL depth (Fig. 5), which is relatively symmetric about the equator, the seasonal variability is much greater over the Northern Hemisphere (NH) extratropics than it is over the Southern Hemisphere (SH) extratropics (Fig. 7). The stronger NH extratropical seasonality is clearly associated with continental areas (Fig. 7) that have by far the greatest seasonal amplitude in PBL depth, with summer-winter differences approaching 1 km. The seasonality over SH extratropical land areas is probably weaker than that over the NH because the SH land areas are smaller and therefore less continental. That said, even the ocean regions at extratropical NH latitudes exhibit significantly stronger PBL depth seasonality than their SH counterparts. This distinction is summarized in a plot of zonally averaged monthly mean PBL depth departures against latitude (Fig. 8). Another feature clearly evident in Fig. 8 is that there is no appreciable contrast in the seasonal phase evident between land and ocean. At all extratropical latitudes over both land and ocean seasonal maxima in PBL depth occur during late summer (Fig. 8) when land and ocean surface temperatures are warmest and static stability is at its lowest.

The extratropical NH maximum in the seasonal amplitude of PBL depth over land occurs at 40-70°N consistent with strong seasonality in solar insolation and land surface temperature. This drives a strong seasonal cycle of static stability, with much lower values during summer, here shown using estimated inversion strength (EIS, Fig. 9, 10 and 11, see section 2.1.3 above). Indeed, high land surface temperatures appear to be the primary determinant of the deeper PBL depth over Europe during summer (Seidel et al. 2012), a finding qualitatively consistent with the COSMIC data. The seasonal amplitude of PBL depth over land decreases further northward of

60-70°N (Fig. 8), a feature also seen, but to a weaker degree, over the SH land areas. This reduction in amplitude is not matched by a weakening EIS seasonality (Fig. 11).

Over both NH and SH extratropical oceans, the PBL depth seasonality is weak between 30 and 50° (Fig. 8) and maximizes at the polar latitudes (>60°). The late summertime maxima in PBL depth over the more poleward extratropical oceans have been observed in wind profiler data at a coastal site in Denmark (Peña et al. 2012), and can be seen in the radiosonde data at Macquarie Island and at St. Paul Island (Fig. 4). Analysis of sounding data from the Azores in the north Atlantic at 40°N shows that the seasonal maximum PBL depth occurs during winter (Rémillard et al. 2012). This is more in line with subtropical behavior (see section 3.2 below). The late summertime maximum in extratropical ocean PBL depth occurs at the same times as the sea-surface temperature (SST) maximizes (not shown). Extratropical oceans poleward of 60° exhibit reduced EIS during summertime (Fig. 11) but the seasonal phase of EIS equatorward of 60° varies strongly with latitude. Over the Southern Ocean between 40-60°S, EIS maximizes during early summer, and the PBL depth maximizes during mid-late summer. Several studies have identified negative correlations between LTS/EIS and PBL depth (e.g. Wood and Hartmann 2006, Lin et al. 2009) for subtropical and tropical clouds. Here, we are noting a positive correlation for the seasonality of PBL depth and EIS for 40-60°S.

Why is there a positive PBL depth-EIS correlation in the seasonal cycle over the Southern Ocean? By itself, increased EIS would be expected to drive summertime minima in PBL depth by suppressing the growth of the PBL by entrainment, as happens over the subtropical northeastern Pacific (see section 3.2 below and Lin et al. 2009). However, in addition to a dependence upon static stability, the depth of the PBL is also controlled by surface fluxes (Medeiros et al. 2005), large-scale subsidence, and the efficiency of PBL radiative cooling.

Surface fluxes are greater during wintertime primarily due to the larger sea-air temperature difference. Mean vertical motion in the extratropical lower troposphere over the Southern Ocean is also upward during wintertime and approximately zero during summertime, and so it is difficult to see how this would drive summertime maxima in PBL depth.

The most likely reconciliation is that the higher PBL tops observed with COSMIC on average during summer are most likely caused by more frequent summertime detection of the tops of moist layers during periods of warm advection. During wintertime, warm advection tends to be more commonly associated with strong synoptically-driven ascent producing warm conveyor belts with no discernible hydrolapse (Norris 1998), whereas with the storm track having migrated poleward, summertime warm advection more frequently occurs during conditions of weaker or even no ascent, stunting vertical transport of moisture. This likely produces hydrolapses that may be readily detected by COSMIC. While well-capped stratocumulus is common during summer and winter over the extratropical oceans, it is the warm advective fair weather cloud types (stratus and fog) that together are significantly more common during summertime (Norris 1998). Norris shows, from an analysis of sounding data over the North Atlantic (53°N, 36°W), that the hydrolapse atop summertime fair weather stratus clouds occurs at ~850 hPa on average, whereas summertime stratocumulus is capped by a hydrolapse around 900 hPa. In contrast, wintertime stratocumulus extends higher to ~850 hPa. Therefore, summertime stratocumulus over the extratropical oceans appears to be confined to a shallower PBL, but the frequent existence of warm advective PBLs extending higher during the summer may compensate. The key question needed to understand the seasonality of the COSMIC-determined PBL depth over the Southern Ocean is what determines the height of the hydrolapse during periods of warm advection. Addressing this question is beyond the scope of this study, but factors such as the slope of the isentropes and the meridional distance of the storm track from the edge of the Ferrell-Hadley cell boundary are likely contributing factors worthy of exploration in future studies.

3.2 Subtropical/tropical seasonal variability

At tropical/subtropical latitudes, the seasonal phase of the PBL depth is almost opposite that at extratropical latitudes (Fig. 8). The seasonal amplitudes are also more symmetrical about the equator than is the case at extratropical latitudes. The seasonal amplitude is not zonally symmetric but maximizes at longitudes of the primary monsoon circulations — Southeast Asia and the maritime continent, North. Africa, the tropical Americas — and weakens away from the monsoonal centers of action (Fig. 7). In these regions, most notably in the NH, the PBL depth maximizes during the dry winter season and minimizes during the summer monsoon season. Indeed, the seasonal march of the minimal PBL depth migrates north and south following the ITCZ (Fig. 8). Land areas exhibit this seasonality most clearly (Fig. 8b).

The tendency for maximal tropical/subtropical PBL depths during the dry season may be explained by an argument involving the Bowen ratio. During the wet season, more of the surface solar heating is used to evaporate water, whereas during the dry season, greater surface sensible heat flux is available to drive vertical dry mixing. Although latent heating can also drive mixing by producing buoyant cloudy thermals, in the wet season these primarily vent mass *out* of the PBL because thermals are frequently sufficiently strong to penetrate the PBL inversion because of the lower static stability (Figs. 10 and 11) and moisture convergence associated with the monsoonal low level flow. The stronger subsidence associated with the downward branches of the Hadley circulation also caps the inversion so that surface-driven thermals in dry zones remain within the PBL. Thus, over the subtropical/tropical land area, the PBL depth is not dictated by the seasonal cycle in EIS (compare Fig. 8 with Figs. 10 and 11) but by the availability of surface moisture.

Over the subtropical/tropical SH oceans (Fig. 8a) the peak PBL depth is shifted to late Austral fall (MAM) and the minimum in late spring (SON). The Austral fall maximum in the zonal mean annual cycle is primarily driven by the southeastern subtropical Pacific Ocean and Atlantic Ocean cycles with other subtropical/tropical ocean regions contributing relatively weakly to the zonal mean seasonality (Fig. 7b). The seasonal maxima of lower tropospheric static stability occur earlier (springtime) over the SH subtropical eastern oceans compared with summertime maxima over their NH counterparts (Klein and Hartmann 1993). This is most likely due to the greater importance of orographic blocking of midlatitude westerly flow over the SH (Richter and Mechoso 2006), which drives earlier EIS maxima (Fig. 10) since midlatitude westerlies are stronger. A key climatic consequence is that the anomalously shallow PBLs during SON support maxima in southeastern Pacific stratocumulus cloud cover during these seasons, whereas cloud cover maxima over the northeastern Pacific occur closer to the summer solstice (see Fig. 7 in Wood, 2012, see also Lin et al. 2009).

4 Relative importance of moisture and temperature jumps to COSMIC-detected PBL top

As discussed in section 2.2, GPS-RO is sensitive to vertical gradients in refractivity *N*. The vertical gradient of refractivity atop the PBL is uniquely determined by gradients in pressure, temperature and water vapor pressure, which may be expressed mathematically by taking the vertical derivative of Eqn. [1]:

$$N' = \frac{dN}{dz} = a\frac{p'}{T} - \left(a\frac{p}{T^2} + 2b\frac{p_w}{T^3}\right)T' + b\frac{p_w'}{T^2} \qquad [2]$$

Because pressure is a smoothly varying function of height, the p' term does not contribute significantly to PBL top detection, although its slow variation does provide a ‘background’ N' value of 20-30 N-units km^{-1}, with variations in the p'term driven by temperature alone. The two terms involving $T'$and p_w' contribute to the detection of PBL tops, for which $N' < -50$ N-units km^{-1} (see section 2.2 above). To examine the relative contributions of $T'$and p_w' to N' for successfully-detected PBL tops we produce composite vertical profiles of T, $p_w$and the T', p_w' terms in Eqn. [2] as a function of a height coordinate $z_* = z–h$ that is defined to be zero at the height h of the detected PBL top. These are shown in Fig. 12 for four of the stations encompassing a wide range of latitudes (Hong Kong, Hilo, Macquarie Island and Halley). Table 4 provides a summary of the mean values of the minima in the $T'$and p_w' terms in Eqn. 2 and in $T'$and p_w' themselves.

The results of the composite analysis show that, for the tropical and subtropical sites, the moisture gradient contribution to the refractivity jump is more than an order of magnitude greater than the temperature gradient contribution. This is despite a significant temperature inversion (see Fig. 12 and Table 4) accompanying the detected PBL tops. Only at Halley on Antarctica, with its much colder temperatures (255 K at the inversion base in the mean) and consequently lower water vapor pressures, does the temperature jump contribute more than the moisture jump. These findings confirm that over most of the globe, it is the hydrolapse atop the PBL that our PBL top determination algorithm is detecting.

5 PBL sharpness

In the study of PBL top detection from COSMIC by Ao et al. (2012), a sharpness parameter S is introduced that compares, for a given profile, the ratio of the *minimum* value of the refractivity gradient N' in the profile to the *mean* value of N' over the lowest 6 km of the atmosphere, i.e. S = $\min[N']\,/\overline{N'}$ to. We obtain the sharpness parameter using all profiles extending below 500 m, not only those for which a PBL top has been detected. Figures 13 and 14 show the annual mean sharpness and the seasonal departures of the mean sharpness from the annual mean. Sharpness is greatest in regions with a high frequency of PBL top detection (compare Fig. 13 with Fig. 2).This is not too surprising since a sharpness criterion is used in the PBL top detection algorithm (section 2.2). However, it is still useful to examine quantitatively the degree of sharpness and its seasonality.

High values of sharpness ($S > 2$) occur over the subtropics, especially over the cold eastern subtropical oceans west of the major continental landmasses, where values each as high as 3 (Fig. 13). Low value of sharpness parameter ($S < 2$) occur in polar regions and in the warm Tropics, but note that only over the poles does the mean sharpness fall as low as 1.5. Low sharpness is likely a result of multiple hydrolapses in the tropics and extratropics, but temperature might play a significant role in polar regions (see section 4). Seasonal variations of the sharpness parameter follow the seasonal anomalies in PBL depth (compare Fig. 14 and Fig. 7) but the seasonal anomalies of S are stronger in the subtropics/tropics than they are in the extratropics. The anomalies are most pronounced during DJF and JJA. Poleward of 40°, negative anomalies occur during winter and positive anomalies during summer. In contrast, the seasonal cycle is opposite in the subtopics/tropics.

6 Discussion and Conclusions

The depth of the planetary boundary layer (PBL), deduced here from spaceborne GPS radio occultation as the level with a particularly strong vertical refractivity gradient, has a distinct seasonal cycle in most locations. As we discuss in section 3, the seasonal cycle is dramatically different within the subtropics/tropics from that in the extratropics. Late summertime maxima prevail in the extratropics. Over land, the summertime maxima are driven largely by surface heating and reduced static stability, while over the ocean the summertime maxima may be associated with warm advection of shallow moist layers from the tropics. In contrast, maxima within the subtropical/tropical belt largely occur during the dry season (winter) most likely driven by seasonally-strong surface sensible heat fluxes, with suppressed PBL vertical development during the rainy seasons, an assessment that provides support for the analysis of PBL depth in a global model by Medeiros et al. (2005).

What are the consequences of the seasonal march of PBL depth? First, as numerous studies over polluted continental areas have shown, reduced mixing during winter makes it difficult to disperse atmospheric pollutants and can results in more serious aerosol pollution events. PBL depth is also an important determinant of cloud type and therefore albedo (Wood and Bretherton 2004). Over the cool subtropical oceans, cloud cover increases as the PBL depth decreases because the capping inversion atop the PBL serves as a constraint on the vertical transport of moisture, keeping the relative humidity high in the PBL and encouraging clouds (Wood and Hartmann 2006). Therefore, the seasonal march of PBL depth seen here over the subtropical eastern oceans is in phase with the seasonal cycle of cloud cover (e.g. Klein and Hartmann 1993). That said, over the extratropical oceans, the seasonal cycle of PBL depth deduced from COSMIC appears to be somewhat out of phase with the stability, an issue that will need further investigation in future studies.

The robust seasonality of the PBL depth as deduced by COSMIC should provide an important constraint on the behavior of global models, particularly because the close connection between PBL depth and cloud properties may provide new insights into the behavior of low clouds in models. The extent to which models can reproduce the patterns of seasonal PBL depth variability seen in Figs. 7 and 8 would provide new confidence in the ability of models to respond appropriately to changes in stability and surface heating. These are responses that will prove central to how the atmosphere responds to climate changes and so a new seasonal PBL climatology like the one described here should be used to confront models in future work.

Acknowledgements

The authors would like to thank Feiqin Xie, Chi Ao, Dong Wu, Anthony Mannucci and Joao Teixeira for discussions about the GPS Radio Occultation dataset. The authors acknowledge the COSMIC Data Analysis and Archive Center (CDAAC) for provision of the COSMIC GPS RO soundings. Radiosonde data were obtained from the Stratospheric Processes and their Role in Climate (SPARC), the British Atmospheric Data Centre (BADC) and the University of Wyoming. We thank Larry Oolman at the University of Wyoming for providing the Hong Kong radiosonde dataset.

5. References

Albrecht, B. A., M. P. Jensen, and W. J. Syrett, 1995: Marine boundary layer structure and fractional cloudiness. *J. Geophys. Res*., 100 (D7), 14209–14222.

Anthes, R. A., and Coauthors, 2008: The COSMIC/FORMOSAT-3 mission: Early results. Bull. Amer. Meteor. Soc., 89, 313–333.

Ao, C. O., D. E. Waliser, S. K. Chan, J.-L. Li, B. Tian, F. Xie, and A. J. Mannucci (2012), Planetary boundary layer heights from GPS radio occultation refractivity and humidity profiles, J. Geophys. Res., 117, D16117, doi:10.1029/2012JD017598.

Arya, S. P., 2009: Introduction to Micrometeorology Second Edition.

Bean, B. R., and E. J. Dutton, 1968: Radio Meteorology. Dover, 435 pp.

Caldwell, P., C. S. Bretherton, and R. Wood, 2005: Mixed layer budget analysis of stratocumulus dynamics during EPIC. *J. Atmos. Sci.*, **62**, 3775-3791.

Dima, I. M., J. M. Wallace, 2003: On the seasonality of the Hadley cell. *J. Atmos. Sci.*, **60**, pp. 1522-1527.

Guo, P., Y.-H. Kuo, S. V. Sokolovskiy, D. H. Lenschow, 2011: Estimating Atmospheric Boundary Layer Depth Using COSMIC Radio Occultation Data. J. Atmos. Sci., 68, 1703–1713.

Hande, L. B., S. T. Siems, M. J. Manton, and D. Belusic (2012), Observations of wind shear over the Southern Ocean, J. Geophys. Res., 117, D12206, doi:10.1029/2012JD017488.

Hajj, G. A., and Coauthors, 2004: CHAMP and SAC-C atmospheric occultation results and intercomparisons. *J. Geophys. Res.*, **109,** D06109, doi:10.1029/2003JD003909.

Heck, P. W., B. J. Byars, D. F. Young, P. Minnis, and E. F. Harrison, 1990: A climatology of satellite derived cloud properties over marine stratocumulus regions. Preprints, *Conf. on Cloud Physics*, San Francisco, CA, Amer. Meteor. Soc., J1–J7.

Karlsson, J., G. Svensson, S. Cardoso, J. Teixeira, S. Paradise, 2010: Subtropical Cloud-Regime Transitions: Boundary Layer Depth and Cloud-Top Height Evolution in Models and Observations. *J. Appl. Meteor. Climatol.*, **49**, 1845–1858.

Klein, S. A., and D. L. Hartmann, 1993: The seasonal cycle of low stratiform clouds. *J. Clim.*, **6**, 1587-1606.

Kursinski, E. R., 1997: Observing Earth's atmosphere with radio occultation measurements using the Global Positioning System. *Journal of Geophysical Research*, **102** (d19), p. 23429.

Lin, W, M. Zhang, N. G. Loeb, 2009: Seasonal Variation of the Physical Properties of Marine Boundary Layer Clouds off the California Coast. J. Climate, 22, 2624–2638.

McGrath-Spangler, E. L., and A. S. Denning (2012), Estimates of North American summertime planetary boundary layer depths derived from space-borne lidar, J. Geophys. Res., 117(D15101), doi:10.1029/2012JD017615.

McGrath-Spangler, E. L., and A. S. Denning (2013), Global seasonal variations of midday planetary boundary layer depth from CALIPSO space-borne LIDAR, J. Geophys. Res. Atmos., 118, doi:10.1002/jgrd.50198.

Medeiros, B., A. Hall, B. Stevens, 2005: What Controls the Mean Depth of the PBL?. J. Climate, 18, 3157–3172.

Minnis, P., P. W. Heck, D. F. Young, C. W. Fairall, and J. B. Snider, 1992: Stratocumulus cloud properties derived from simultaneous satellite and island-based instrumentation during fire. *J. Appl. Meteor.*, **31,** 317–339.

Norris, J. R., 1998: Low Cloud Type over the Ocean from Surface Observations. Part I: Relationship to Surface Meteorology and the Vertical Distribution of Temperature and Moisture. *J. Climate*, **11**, 369–382.

Palm, S. P., A. Benedetti, and J. Spinhirne (2005), Validation of ECMWFglobal forecast model parameters using GLAS atmospheric channel measurements, Geophys. Res. Lett., 32(22), L22S09, doi:10.1029/2005GL023535.

Randall, D. A., Q. Shao, and M. Branson (1998), Representation of clear and cloudy boundary layers in climate models, in Clear and Cloudy Boundary Layers, edited by A. A. M. Holtslag, and P. G. Duynkerke, pp. 305–322, Royal Netherlands Academy of Arts and Sciences, Amsterdam.

Rémillard, J., P. Kollias, E. Luke, R. Wood, 2012: Marine Boundary Layer Cloud Observations in the Azores. J. Climate, 25, 7381–7398.

Richter, I., C. R. Mechoso, 2006: Orographic Influences on Subtropical Stratocumulus. *J. Atmos. Sci.*, **63**, 2585–2601.

Seidel, D. J., C. O. Ao, and K. Li (2010), Estimating climatological planetary boundary layer heights from radiosonde observations: Comparison of methods and uncertainty analysis, J. Geophys. Res., 115, D16113, doi:10.1029/2009JD013680.

Seidel, D. J., Y. Zhang, A. C. M. Beljaars, J.-C. Golaz, A. R. Jacobson, and B. Medeiros (2012), Climatology of the planetary boundary layer over the continental United States and Europe, J. Geophys. Res., 117, D17106, doi:10.1029/2012JD018143.

Sokolovskiy, S. V., 2001a: Modeling and inverting radio occultation signals in the moist troposphere. *Radio Sci.,* **36,** 441–458.

Sokolovskiy, S. V., 2003: Effect of superrefraction on inversions of radio occultation signals in the lower troposphere. *Radio Sci.,* **38,** 1058, doi:10.1029/2002RS002728.

Sokolovskiy, S., Y.-H. Kuo, C. Rocken, W. S. Schreiner, D. Hunt, and R. A. Anthes (2006), Monitoring the atmospheric boundary layer by GPS radio occultation signals recorded in the open-loop mode, Geophys. Res. Lett., 33, L12813, doi:10.1029/2006GL025955.

Stull, B. R., 1988: An Introduction to Boundary Layer Meteorology.

Tackett, J. L., and L. Di Girolamo (2009), Enhanced aerosol backscatter adjacent to tropical trade wind clouds revealed by satellite-based lidar, Geophys. Res. Lett., 36, L14804, doi:10.1029/2009GL039264.

von Engeln, A., J. Teixeira, J. Wickert, and S. A. Buehler (2005): Using CHAMP radio occultation data to determine the top altitude of the planetary boundary layer, Geophys. Res. Lett., 32, L06815, doi:10.1029/2004GL022168.

Wood, R., and C. S. Bretherton, 2004: Boundary Layer Depth, Entrainment, and Decoupling in the Cloud-Capped Subtropical and Tropical Marine Boundary Layer. *J. Climate*, **17**, 3576–3588.

Wood, R., and C. S. Bretherton**,** 2006: On the relationship between stratiform low cloud cover and lower tropospheric stability. *J. Clim.,***19**, 6425-6432.

Wood, R., 2012: Stratocumulus Clouds. *Mon. Wea. Rev.*, **140**, 2373–2423.

Wu, D., Hu, Y., McCormick, M., Xu, K., Liu, Z., Smith, B., Omar, A., and Chang, F.: Deriving marine-boundary-layer lapse rate from collocated CALIPSO, MODIS, and AMSR-E datato study global low-cloud height statistics, Geosci. Remote Sens. Lett., 5, 649–652, 2008.

Wyant, M. C., R. Wood, C.S. Bretherton, C. R. Mechoso, J. Bacmeister, M. A. Balmaseda, B. Barrett, F. Codron, P. Earnshaw, J. Fast, A. Hall, C. Hannay, J. W. Kaiser, H. Kitagawa, S. A. Klein, M. Koehler, J. Manganello, H.-L. Pan, S. Wang, and Y. Wang, 2010: The PreVOCA Experiment: Modeling the lower troposphere in the Southeast Pacific**.** *Atmos. Chem. Phys.,* **10**, 4757-4774, doi:10.5194/acp-10-4757-2010.

Xie, F., Wu, D. L., Ao, C. O., Mannucci, A. J., and Kursinski, E. R.: Advances and limitations of atmospheric boundary layer observations with GPS occultation over southeast Pacific Ocean, Atmos. Chem. Phys., 12, 903-918, doi:10.5194/acp-12-903-2012, 2012

Yunck, TP (2000). "A history of GPS sounding". TAO : Terrestrial, atmospheric, and oceanic sciences (1017-0839), 11 (1), p. 1.

Zuidema, P., D. Painemal, S. de Szoeke, C. Fairall. (2009) Stratocumulus Cloud-Top Height Estimates and Their Climatic Implications. *Journal of Climate* **22**:17, 4652-4666

Table 1. Details of the radiosonde stations used in this study.

Station	**Longitude**	**Latitude**	**Region**	**Dataset source**	**Vertical resolution (approx, m)**	**Years analyzed**
St. Paul Island, Alaska	170.2°W	57.2°N	Bering Sea	SPARC	~30	2006-2008
Annette, Alaska	131.6°W	55.0°N	Gulf of Alaska	SPARC	~30	2006-2008
Hong Kong, China	114.2°E	22.3°N	Southern China	UWYO	~200	2006-2010
Hilo, Hawaii	155.0°W	19.7°N	Tropical Pacific	SPARC	~30	2006-2008
Macquarie Island, Australia	158.9°E	54.5°S	Southern Ocean	BADC	~50	2006-2009
Halley, Antarctica	26.7°W	75.6°S	Weddell Sea	BADC	~50	1995-2011

Table 2. Annual mean PBL depth from COSMIC and radiosonde estimates and difference between them.

Station	**Annual Mean PBL depth [km]**		
	COSMIC	**radiosonde**	**difference**
St. Paul Island, Alaska	1.30	1.29	0.01
Annette, Alaska	1.41	1.50	-0.09
Hong Kong, China	1.64	1.92	-0.28
Hilo, Hawaii	1.85	2.07	-0.22
Macquarie Island	1.34	1.20	0.14
Halley, Antarctica	0.84	0.79	-0.05

Table 3: Maximum absolute monthly anomalies (|monthly mean – annual mean|) in PBL depth and the months of max and min PBL depth from the COSMIC and radiosonde data, and the correlation coefficient between the COSMIC and radiosonde seasonal cycles.

Station	**Maximum absolute seasonal anomaly in PBL depth [km] and month of [max/min]**		
	COSMIC	**Radiosonde**	***r* between seasonal cycles**
St. Paul Island, Alaska	0.24 [Oct/Mar]	0.30 [Aug/Mar]	**0.77**
Annette, Alaska	0.15 [Oct/May]	0.19 [Mar/Jan]	0.35
Hong Kong, China	0.50 [Jan/Jul]	0.61 [Jan/Jul]	**0.61**
Hilo, Hawaii	0.22 [Oct/Dec]	0.32 [Aug/Nov]	0.39
Macquarie Island	0.08 [Mar/May]	0.09 [Mar/Jul]	**0.69**
Halley, Antarctica	0.29 [Jan/Aug]	0.35 [Dec/Aug]	**0.82**

Table 4: Means of the minimum values of the gradients in refractivity, temperature and water vapor pressure occurring the top of successfully-diagnosed PBLs at four radiosonde stations.

Station	**Mean T at inversion base [K]**	**Mean p_w at inversion base [hPa]**	**Mean values of minima from all soundings with diagnosed PBL**		
			$\langle \min N' \rangle$ [N-units km^{-1}]	**$\langle \min T' \text{ term} \rangle$[1] [$N$-units km^{-1}]** $\langle max\, T' \rangle$ [K km^{-1}]	**$\langle \min p_w' \text{ term} \rangle$[1] [$N$-units km^{-1}]** $\langle min\ \ p_w' \rangle$ [hPa km^{-1}]
Hong Kong	286	13	**−146**	**−7.1** *6.5*	**−112** -24
Hilo, Hawaii	284	11	**−210**	**−5.0** *6.5*	**−180** *−38*
Macquarie Island	270	4.2	**−81**	**−3.8** *10.2*	**−45** *−9.8*
Halley, Antarctica	255	1.3	**−67**	**−18.3** *17.9*	**−9.6** *−2.2*

[1] Terms on RHS of Equation [2]

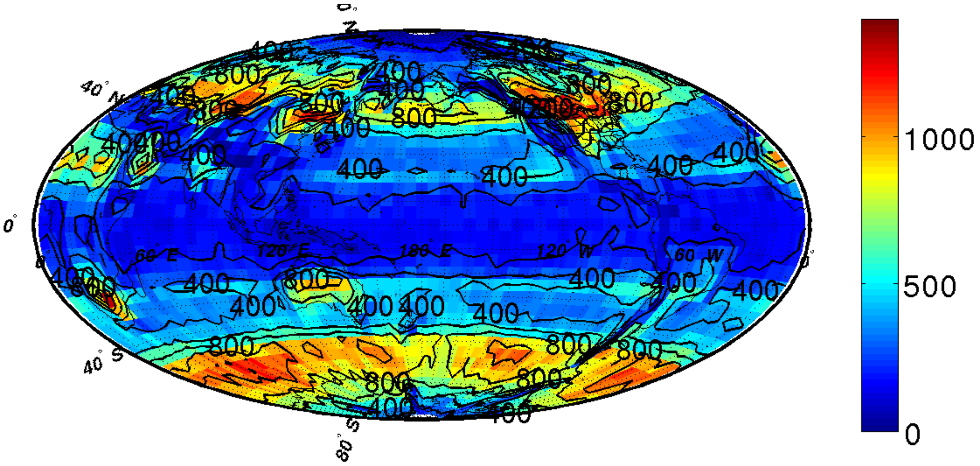

Figure 1. The number of COSMIC GPS-RO retrievals during 2007-2011 for which the signal penetrates to below 500 m above the surface.

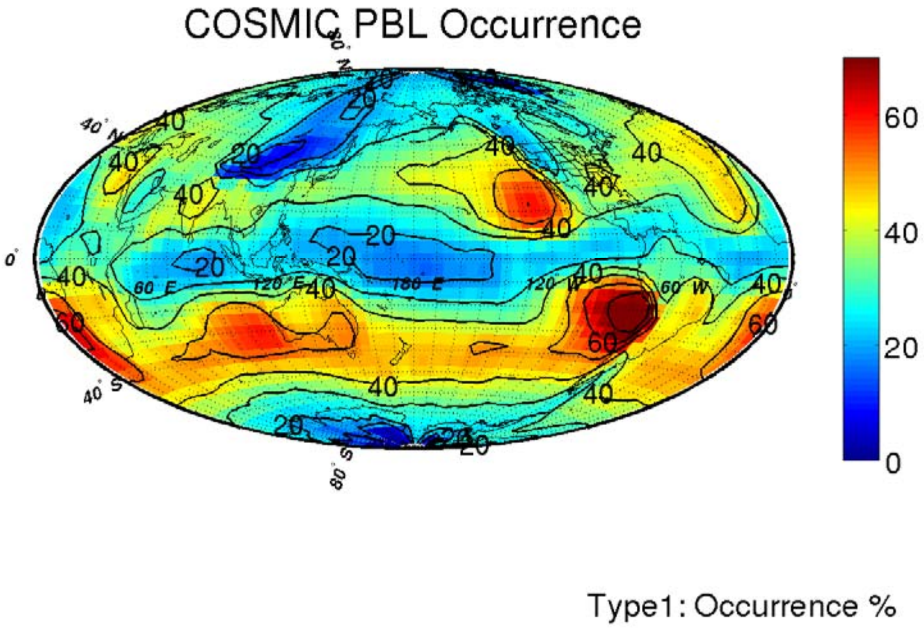

Figure 2. The 2007-2011 annual mean PBL detection frequency, defined as the percentage of profiles extending below 500 m above the surface for which a PBL top is detected.

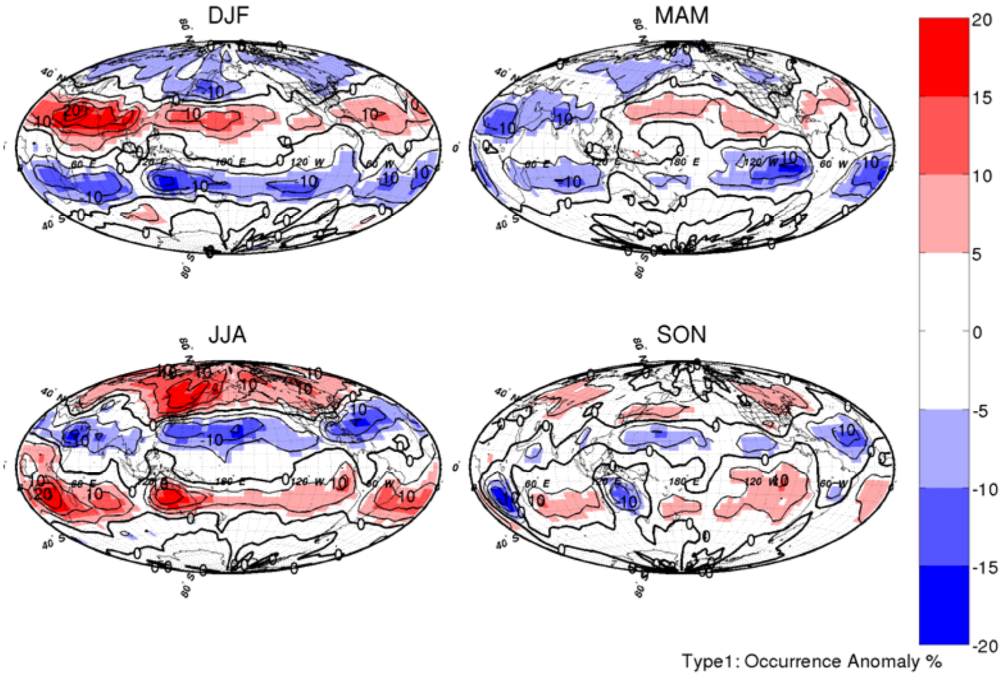

Figure 3: Seasonal anomalies of PBL detection frequency (seasonal frequency – annual frequency).

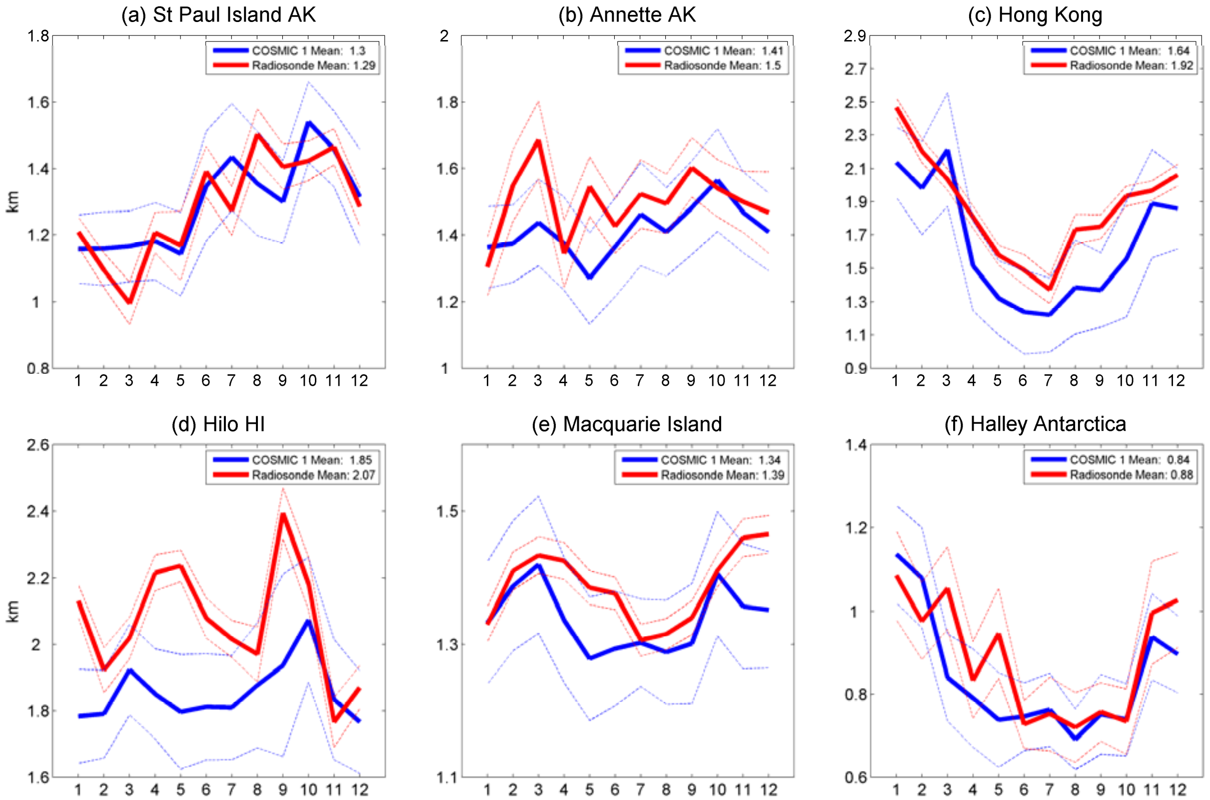

Figure 4. Seasonal cycles (month shown on abscissa) of PBL depths derived from COSMIC (blue) and radiosondes (red) for the six sites described in Table 1. The thick lines are the monthly mean PBL thickness and the dashed lines are the 1-σ standard error in the mean.

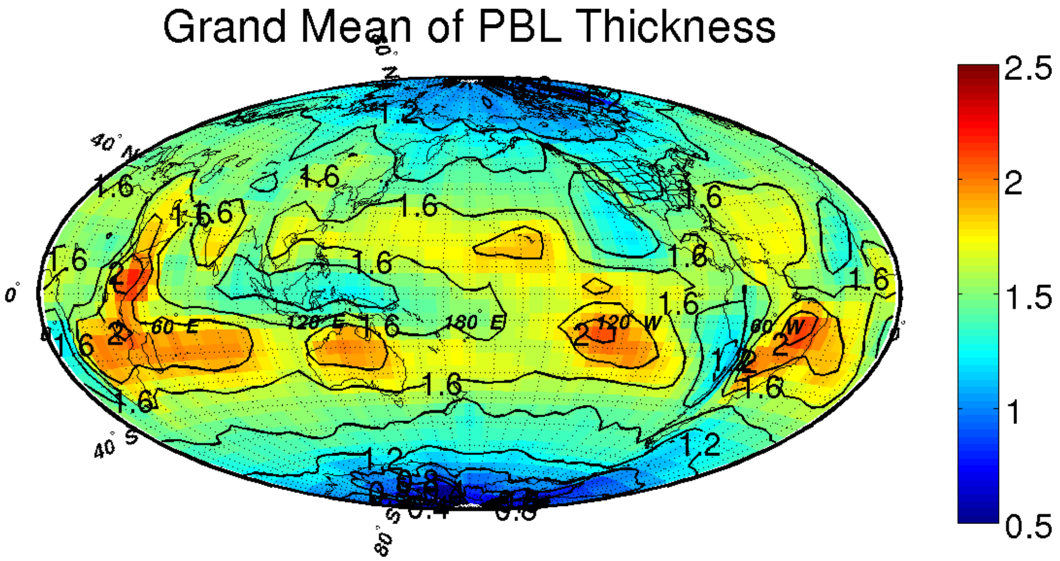

Figure 5: Map of the 2007-2011 annual mean PBL depth [in km] from COSMIC. The thickness over land is shown relative to the terrain height.

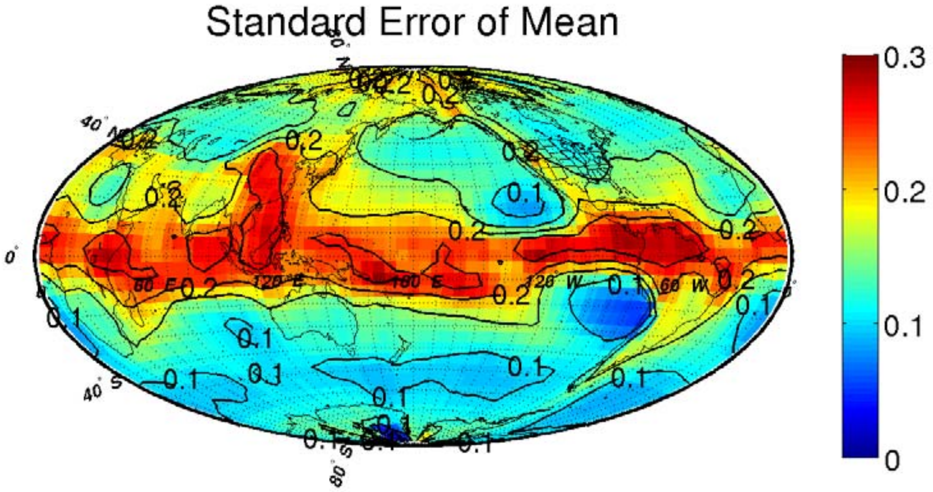

Figure 6: Map of the standard error of the annual mean PBL depth [km] for 2007-2011 from COSMIC.

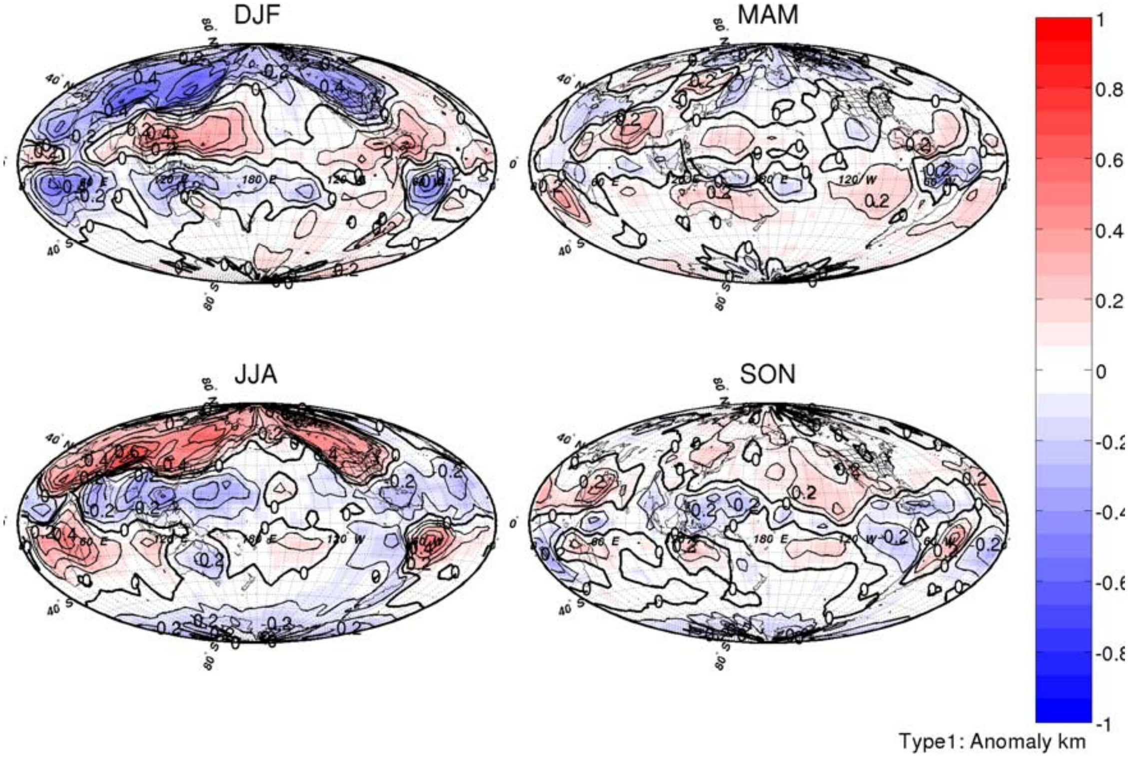

Figure 7. Maps of 2007-2011 seasonal composite PBL depth anomalies [in km] from COSMIC.

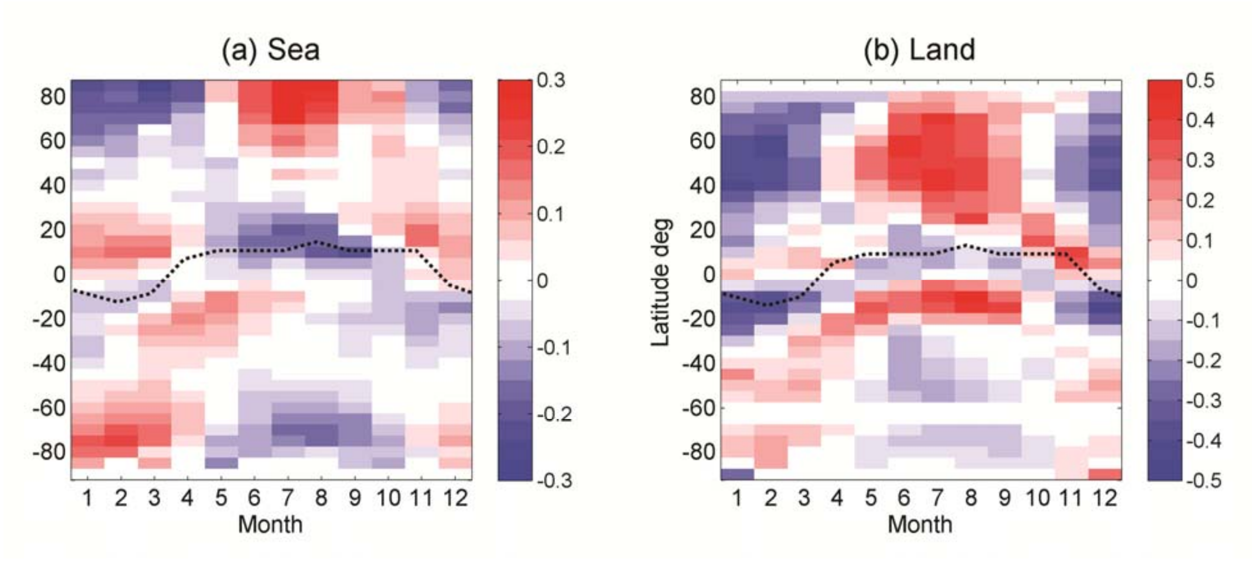

Figure 8: Monthly zonal mean composite PBL depth departures from annual mean over the (a) sea; (b) land. Note the different color scales for the sea and land panels, which have been imposed to facilitate readability because the seasonal amplitudes over land are significantly stronger than those over ocean. The latitude of the marine and continental zonal mean precipitation maximum is shown on each panel (dashed black line)

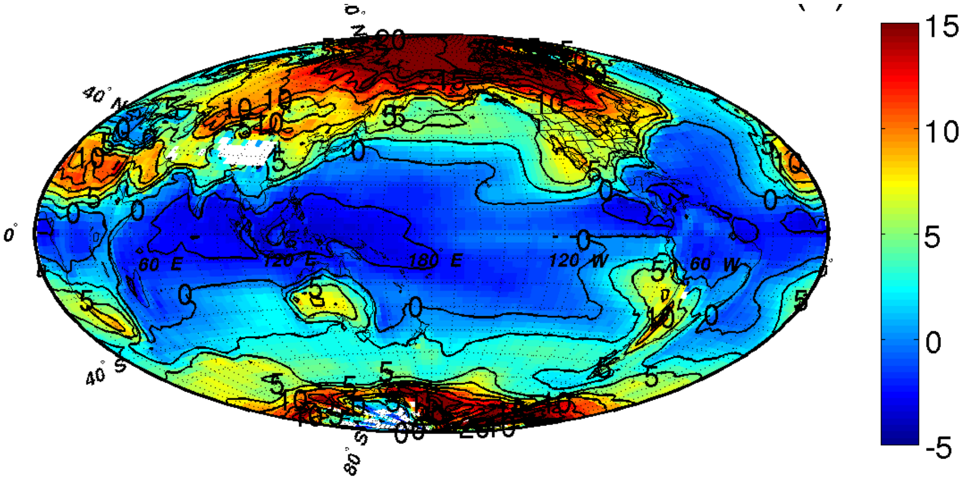

Figure 9: Annual mean estimated inversion strength (EIS) derived from NCEP reanalysis data for 2007 to 2011.

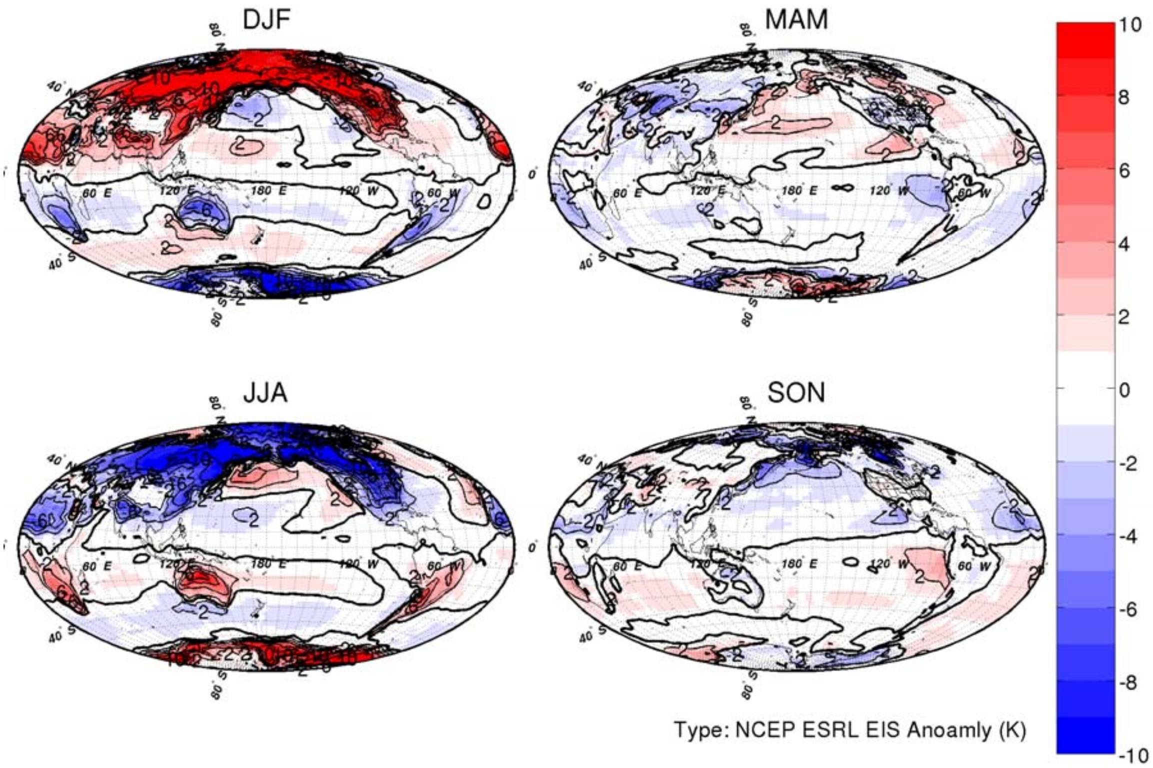

Figure 10: Maps of 2007-2011 seasonal composite anomalies in estimated inversion strength (EIS)

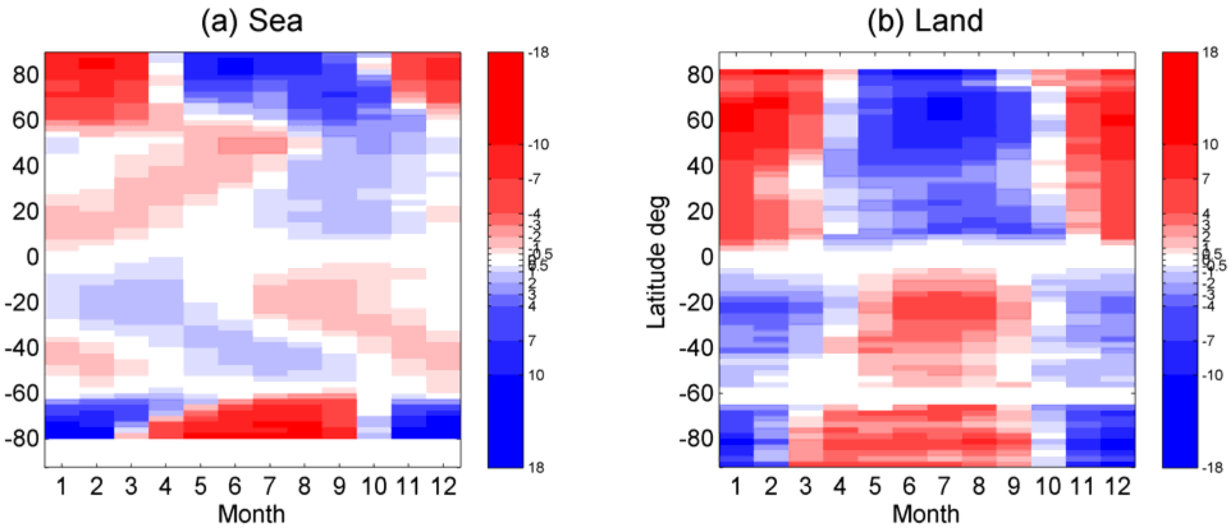

Figure 11: Monthly zonal mean composite EIS departures from annual mean for locations over the (a) sea; (b) land.

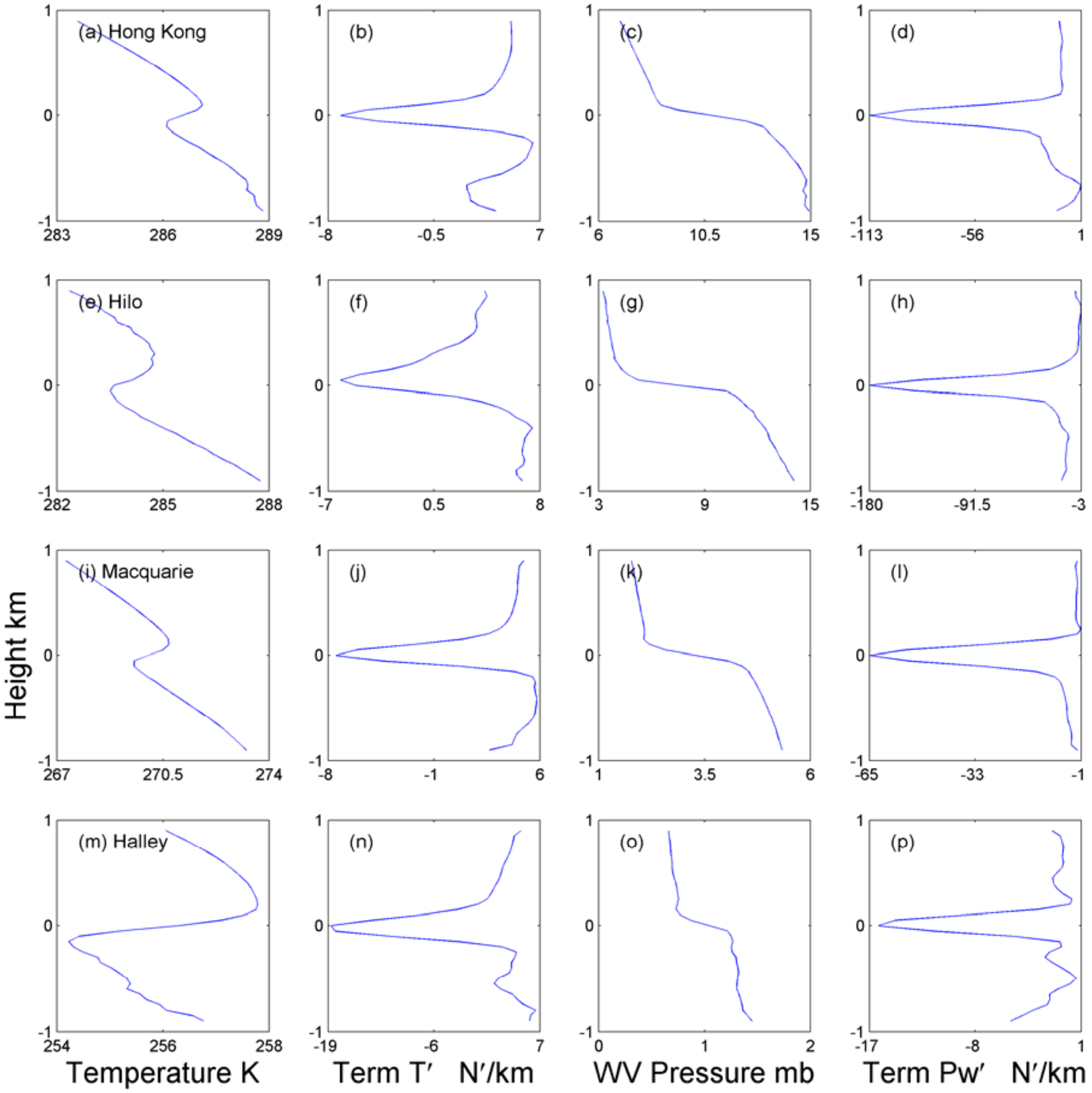
(a) Hong Kong
(b)
(c)
(d)
(e) Hilo
(f)
(g)
(h)
(i) Macquarie
(j)
(k)
(l)
(m) Halley
(n)
(o)
(p)
Height km
1
0
-1
283
286
289
-8
-0.5
7
6
10.5
15
-113
-56
1
282
285
288
-7
0.5
8
3
9
15
-180
-91.5
-3
267
270.5
274
-8
-1
6
1
3.5
6
-65
-33
-1
254
256
258
-19
-6
7
0
1
2
-17
-8
1
Temperature K
Term T′ N′/km
WV Pressure mb
Term Pw′ N′/km

Figure 12: Composite profiles of T (left column), T' term in Eqn. 2 (second column), p_w(third column) the p_w' term in Eqn. 2 (right column) for the successfully-detected PBLs for Hong Kong (top row), Hilo (second row), Macquarie Island (third row), and Halley (bottom row), plotted as a function of the height normalized with the height of the PBL top. Note the change in horizontal scales from row to row.

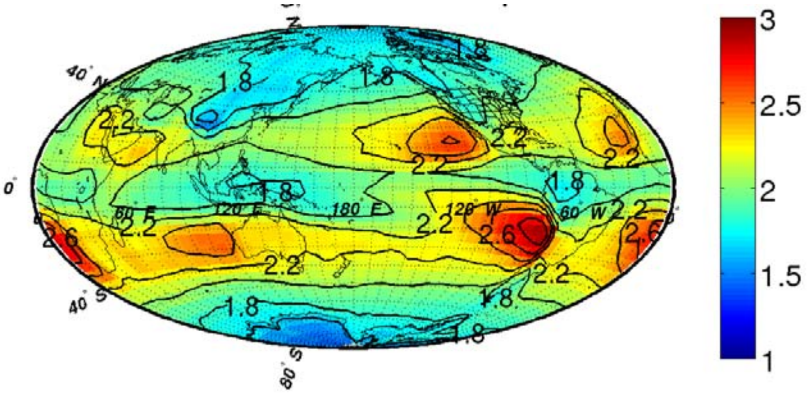

Figure 13. Annual mean refractivity sharpness parameter *S* for 2007-2011. High values indicate a PBL top that is readily distinguishable from other refractivity gradients in the profile, whereas low value indicate a PBL top that is less well-defined.

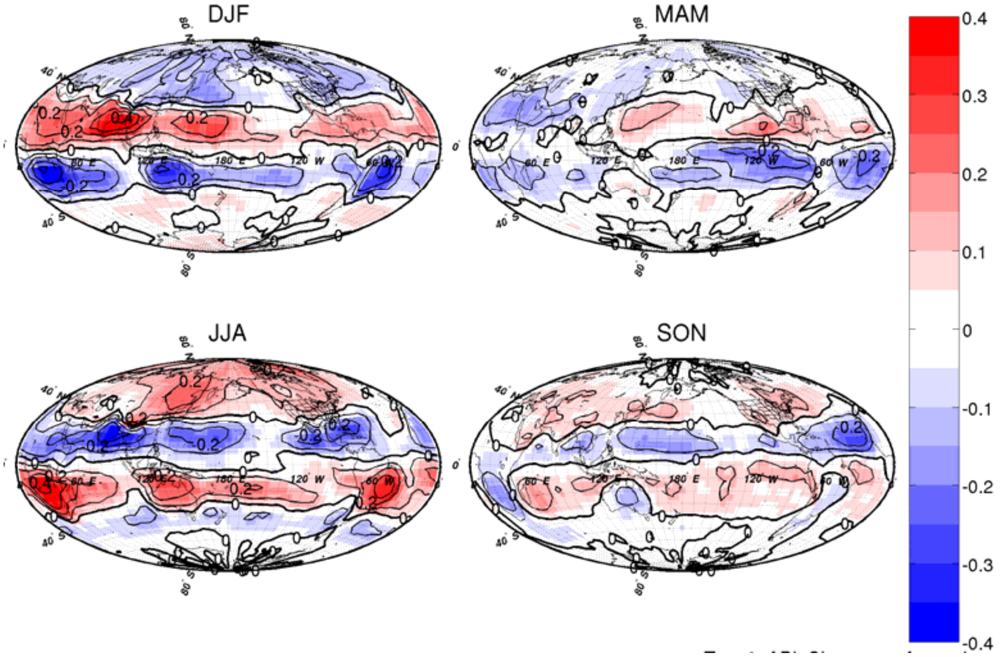

Figure 14. The seasonal composite sharpness parameter anomaly.